Scaling exponents of conductivity-like and resistivity-like Gilbert damping with spin-orbit parameter in oriented hcp Co$_{1-x}$Ir$_x$ soft magnetic films

Sha Zhang,[1,2] Chenhu Zhang,[1] Quanzhi Zhang,[1] Xiaolong Fan,[1] Liang Qiao,[1] Tianyong Ma,[2,3]
Tao Wang,[1,*] Meizhen Gao,[1,†] and Fashen Li[1]

[1]*Institute of Applied Magnetics, Key Laboratory of Magnetism and Magnetic Materials of Ministry of Education,
Lanzhou University, Lanzhou 730000, China*

[2]*Microelectronics and Solid-State Electronics Device Research Center, School of Electrical and Information Engineering,
North Minzu University, Yinchuan 750021, China*

[3]*The Key Laboratory of Physics and Photoelectric Information Functional Materials,
North Minzu University, Yinchuan 750021, China*

Engineering Gilbert damping in ferromagnetic metal films is of great importance to exploit and design spintronic and high-frequency electromagnetic devices. The spin-orbit parameter ξ has been found to be efficient for tuning the Gilbert damping rate α_G in a wide range. However, the theoretically predicted cubic (quadratic) scaling of the conductivity-like α_σ (resistivity-like α_ρ) part of α_G on ξ has not been verified in real ferromagnetic metal materials. To clarify this relationship, herein, we focus on the damping mechanism in oriented hcp Co$_{1-x}$Ir$_x$ soft magnetic films by combining ferromagnetic resonance measurements with first-principle calculations. The α_G is found to increase linearly as the Ir concentration x changes from 0.02 to 0.23, where ξ is dominant over other related parameters. In particular, we demonstrate the $\xi^{2.51}$ ($\xi^{1.69}$) dependence of α_σ (α_ρ) in oriented hcp Co$_{1-x}$Ir$_x$ soft magnetic films by extracting α_σ and α_ρ according to the temperature dependence of α_G, which validates the theoretical prediction. The difference in the ξ dependence of the two types of damping is mainly derived from the non-negligible variation in the density of states at the Fermi surface (D_{Ef}) induced by ξ. The present results provide a deeper insight into the Gilbert damping mechanism and suggest an approach to tailor the magnetic damping freely in magnetic metallic materials.

I. INTRODUCTION

Magnetic damping determines how fast the magnetization relaxes toward the effective magnetic field in magnetization dynamics and plays a central role in many aspects of magnetization switching and dynamics [1,2]. It is usually characterized by the Gilbert damping rate α_G in the Landau-Lifshitz-Gilbert equation [1]. The strength of α_G has a large impact on the speed and energy required to operate spintronic and high-frequency electromagnetic devices [3]. For example, small α_G is essential for minimizing the magnetic switching current and the power consumption in spin-torque-transfer-based magnetic memory devices [4]. Conversely, large α_G is preferred to reduce the reversal time and improve the signal-to-noise ratio in heat-assisted magnetic recording [5]. Therefore, it is desirable to independently optimize α_G in ferromagnetic metal films for a particular application [6]. However, even the intrinsic α_G is challenging to engineer because it is affected by numerous parameters and its physical mechanisms in various ferromagnetic metals have yet to be confirmed [2,3].

Intrinsic Gilbert damping has been thought to arise from the combined effects of spin-orbit (SO) coupling and electron-lattice scattering, and has been treated by various theoretical models, e.g., breathing Fermi surface, torque correlation, and scattering models [7–9]. Accordingly, the impact parameters of α_G include the density of states (DOS) at the Fermi surface (D_{Ef}) [10], SO parameter (ξ) [7], lattice constant, gyromagnetic ratio (γ), saturation magnetization (M_s) [5,11], and electron-lattice scattering rate [7,8]. The first parameter is reported to be a leading factor for determining the α_G of many alloys with almost invariant ξ, such as Fe$_{1-x}$Co$_x$, Co$_{1-x}$Ni$_x$, and Fe$_{1-x}$V$_x$ alloys [10,12,13]. However, D_{Ef} is affected by the details of the band structure near the Fermi surface E_f and, consequently, is difficult to control [3]. By contrast, ξ can be easily controlled, and plays a dominant role in α_G in Fe-, Co-, and Ni-based compounds and alloys with rare-earth elements or 5d metals [7,14,15]. Consequently, ξ can be effectively utilized to engineer α_G. Hence, both theoretical and experimental efforts have been dedicated to determine the dependence of α_G on it [7,14,16].

In theory, Kambersky's torque correlation model partitions Gilbert damping into intraband and interband scattering mechanisms [2,8]. The former (latter) is predicted to decrease (increase) with an increasing electron-lattice scattering rate (proportional to the resistivity ρ), resulting in a conductivity-like α_σ (resistivity-like α_ρ) Gilbert damping rate [7,17]. Based on this model, Gilmore predicted that α_σ and α_ρ are proportional to ξ^3 and ξ^2 in 3d magnetic pure metals, respectively [16]. Experimentally, He *et al.* successfully elucidated the ξ^2

*Corresponding author: wtao@lzu.edu.cn

†Corresponding author: gaomz@lzu.edu.cn

dependence of α_G in $L1_0$ ordered $FePd_{1-x}Pt_x$ films at room temperature where α_ρ was generally dominant over α_σ [7]. However, the scaling exponents of α_σ and α_ρ with ξ have rarely been reported for real ferromagnetic metal materials. The difficulty lies in the fact that the extraction of α_σ and α_ρ is restricted by the existence of extrinsic damping contributions. Moreover, other leading parameters of α_G, such as D_{Ef} and the electron-lattice scattering rate, may have non-negligible and tangled changes, when ξ is tailored by doping or by adjusting the composition ratios in alloys.

In this work, aiming to uncover the ξ dependence of α_σ and α_ρ in real ferromagnetic metals, we study α_G, α_σ, and α_ρ in hcp $Co_{1-x}Ir_x$ soft magnetic films with varying Ir composition x. An hcp $Co_{1-x}Ir_x$ alloy with a prominent intrinsic α_G is selected, as it is expected to have noticeable changes in ξ without additional alterations in D_{Ef} (such as alteration caused by the band filling effect). This is because Ir atoms have ten times larger ξ than Co atoms, but the same number of outer d electrons with Co atoms [18]. Ferromagnetic resonance (FMR) measurements show that α_G increases linearly and the value thereof is tripled by increasing x from 0.02 to 0.23. This tendency generally follows the trend of ξ^2, as, according to the calculation results, ξ dominates the other parameters related to α_G. We then demonstrate approximate cubic (quadratic) scaling of the α_σ (α_ρ) with ξ in the CoIr system by discarding the other effects and separating α_G into α_σ and α_ρ. Our results will contribute to advance the scientific knowledge for magnetic damping, and are expected to facilitate the design and fabrication of new magnetic alloys with tailored damping properties.

II. METHODS

A. Experiment

Direct-current magnetron sputtering with a 0.07-m target-to-substrate distance was employed to prepare c-axis-oriented hcp $Co_{1-x}Ir_x$ ($0.02 \leqslant x \leqslant 0.23$) polycrystalline films in a layered structure: substrate/Ti (8 nm)/Au (25 nm)/CoIr (35 nm)/ Au (2 nm). The Si(100) wafers with oxidized surface were used as substrate. To induce in-plane uniaxial anisotropy, the substrate was inclined using a $15°$ wedge during the sputtering process. The seed and CoIr layers were grown in an Ar atmosphere at 0.15 and 0.25 Pa, respectively. The CoIr layers were grown under 60 W source power by using a Co target with Ir pieces symmetrically placed on an erosion racetrack, which enabled the Ir concentration to be manipulated by changing the number of Ir pieces.

The compositions of the films were determined by energy dispersive x-ray spectroscopy (EDS, Apreo S). The crystalline structures were characterized by x-ray diffraction (XRD, X'Pert PRO with Cu K_α radiation, Philips). The temperature dependence of static magnetic properties was measured by combining a vibrating sample magnetometer (Versalab, Quantum Design) and superconducting quantum interference devices (MPMS XL7 SQUID, Quantum Design). FMR spectra were recorded by a physical property measurement system (PPMS-9, Quantum Design) equipped with a broadband nanoinstrument phaser system (coplanar waveguide FMR system) in the frequency (f) range 6–18 GHz at selected temperatures. For each measurement, an external

magnetic field (H) was swept parallel to the in-plane hard axis of the CoIr film, unless otherwise noted, and the external magnetic field was set up to 40 kOe to magnetize the sample before the measurement. The temperature dependence of electrical resistivities (ρ) was also assessed by a physical property measurement system, with the films patterning into 50-μm-wide Hall bars using standard photolithography and argon ion-milling techniques.

B. Calculation method

Calculations were performed using the full-potential linearized augmented plane-wave method based on density functional theory [19]. The generalized gradient approximation with the Perdew-Burke-Wang form was employed for the exchange-correlation effects [20]. The wave functions were described by spherical harmonics inside the muffin-tin spheres, and by plane waves in the interstitial region. The muffin-tin radius (R_{mt}) of Co (Ir) atoms is 2.20 a.u. (2.32 a.u.). The maximum angular momentum (l_{max}) and the cutoff parameter $R_{MT}K_{MAX}$ were confined to 10 and 7.0, respectively. The band and core-level states were treated with scalar relativistic and fully relativistic effects, respectively. The magnitude of the largest vector in the Fourier expansion of the electron density (G_{max}) was 14.0.

The supercells of $Co_{0.97}Ir_{0.03}$, $Co_{0.94}Ir_{0.06}$, $Co_{0.87}Ir_{0.13}$, $Co_{0.81}Ir_{0.19}$, and $Co_{0.75}Ir_{0.25}$ were identified based on the hcp Co lattice structure ($a = b = 2.458$ Å and $c = 4.033$ Å). For each Ir composition, several doping structures were constructed for the electronic structure calculations. A property (R) involved in this work is the weighted average value according to the probabilities of these structures:

$$R = \sum_{i=1}^{n} P_i R_i, \tag{1}$$

where R_i and P_i are the corresponding calculated property and probability (decided by the total energy) of the ith doping structure, respectively. As an example, details of the calculation of the weighted average value of ξ are provided in the Supplemental Material [21]. The volume and lattice parameters of all the structures were optimized, and the atomic positions in each supercell were fully relaxed until the force on each atom was less than 10.0 mRy/a.u. The k points with a reasonable convergence were set. As an example, for the supercells with a P-$6m2$ structure, the k points were 8000, 30 000, 60 000, 15 000, and 60 000 for $Co_{0.97}Ir_{0.03}$, $Co_{0.94}Ir_{0.06}$, $Co_{0.87}Ir_{0.13}$, $Co_{0.81}Ir_{0.19}$, and $Co_{0.75}Ir_{0.25}$, respectively. SCF calculations with SO coupling parallel to the c axis (z axis) were performed.

III. RESULTS AND DISCUSSION

A. Crystal structure and static magnetic properties

The hcp $Co_{1-x}Ir_x$ ($0.02 \leqslant x \leqslant 0.23$) films have stable crystal structure parameters and equivalent structural qualities. The crystal structure and lattice constant c of the $Co_{1-x}Ir_x$ films were verified by XRD, as shown in Fig. 1(a). Only two peaks can be clearly observed: the (111) peak of
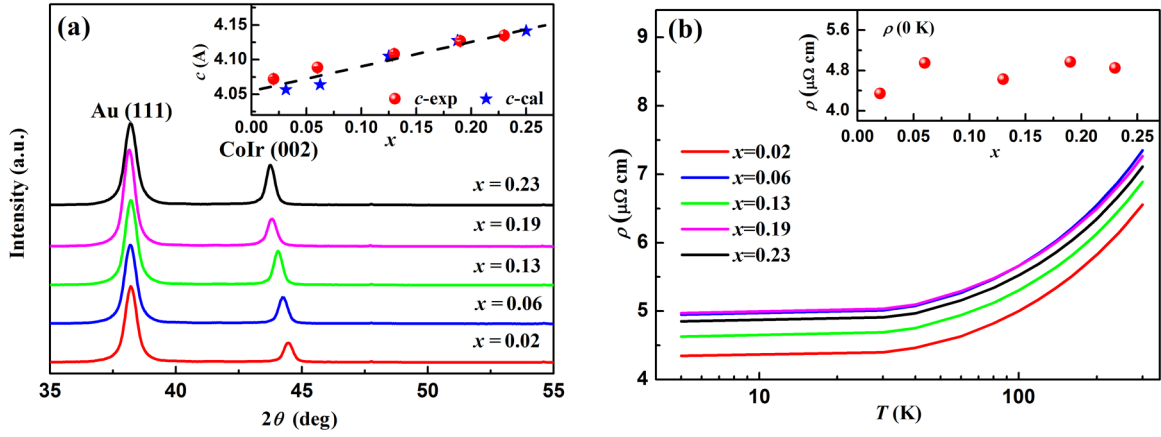
FIG. 1. (a) XRD pattern for the $Co_{1-x}Ir_x$ films. The inset displays the lattice constant c obtained using XRD results (red dots) and first-principles calculations (blue five-pointed stars). The dotted line is drawn for guidance. (b) Temperature dependence of the resistivity ρ for the $Co_{1-x}Ir_x$ films. The inset displays the residual electrical resistivity.

Au and the (002) peak of the CoIr layer. The unique (002) peak reveals that the oriented hcp-CoIr films with their c axes perpendicular to the film plane have been successfully prepared. The (002) peak of $Co_{1-x}Ir_x$ is also observed to shift to smaller diffraction angles with increasing Ir content, according to which the lattice constant c was obtained using the Bragg equation. The lattice constant c is plotted in the inset of Fig. 1(a), which shows that the experimental results are consistent with the calculated ones. The value of c undergoes a slight linear increase as x increases from 0.02 to 0.23; however, in relative terms this increase is only 1.5%, indicating a small and stable lattice expansion.

Figure 1(b) presents the temperature dependence of the electrical resistivity ρ in the $Co_{1-x}Ir_x$ films. The close value and the same behavior of ρ vs temperature for all five samples reflect the similar value and variation of the electron-lattice scattering rate. Apart from this, the $\rho(T)$ determination for a series of $Ti/Au/Co_{0.81}Ir_{0.19}$ $(t)/Au$ films with different thicknesses t ($t = 10 - 120$ nm) and for several Ti (8 nm)/Au (27 nm) films manifests that the ratios of $\rho(T)/\rho(300$ K$)$ for the $Co_{1-x}Ir_x$ films are largely unaffected by the Ti and Au layers. Moreover, the value of the residual electrical resistivity [inset of Fig. 1(b)] remains almost invariant, suggesting the structural quality (similar microstructural defects) of the CoIr samples to be equivalent [2]. This is also evident from the scanning electron microscopy observations (shown in the Supplemental Material [21]).

Stable magnetic structural features should also be expected, considering the high Curie temperature of hcp Co [22,23] The in-plane easy and hard hysteresis loops (examples are shown in the Supplemental Material [21]) confirm that all the films clearly exhibit good soft magnetic properties and in-plane uniaxial anisotropy over the whole measured temperature range. The M_s, conforming to the Bloch law, increases slightly by approximately 2%, when the temperature reduces from 300 to 5 K. According to the fitting results based on Bloch's law [24], at $T = 0$ K, M_s decreases linearly with a relative reduction of about 22% when x increases from 0.02 to 0.23.

B. Gilbert damping α_G

To study the magnetization dynamics, frequency dependent FMR spectra were recorded at $T = 300$ K. (Typical FMR spectra of the $Co_{0.87}Ir_{0.13}$ film are shown in the Supplemental Material [21].) The gyromagnetic ratio γ was obtained by fitting the frequency dependence of the FMR field H_R [25].) Accordingly, the f dependence of ΔH was obtained, and is displayed in Fig. 2. The FMR linewidth ΔH scales linearly with frequency, enabling a precise determination of the measured Gilbert damping parameter α_G from the standard equation [3],

$$\Delta H = \Delta H_0 + \frac{4\pi}{\gamma}\alpha_G f, \qquad (2)$$

where ΔH_0 is the zero-frequency linewidth. From the $\Delta H - f$ fitting, the α_G is obtained and displayed in Fig. 3(a). Obviously, α_G increases linearly with increasing x. Accordingly, we find that the value of α_G at $x = 0$ (0.014) is in agreement with our test result (0.015) using a 35-nm hcp Co film and the reported values (0.018–0.012) [26]. The value of α_G increases from 0.017 to 0.043, corresponding to a 153% relative increment, only by changing x from 0.02 to 0.23. The simple and remarkable linear variation in α_G with the composition provides a convenient way to optimize the damping properties without inducing excessive changes in other magnetic properties, thereby facilitating the interpretations of various effects on α_G.

The measured Gilbert damping α_G consists of intrinsic (α_{int}) and extrinsic damping contributions, wherein the latter is usually caused by two-magnon scattering (TMS), interfacial contributions, radiative damping (α_{rad}), and eddy-current damping (α_{eddy}). However, extrinsic damping is found to constitute only a small proportion (less than 10%). Hence it is negligible as discussed in the following. First, TMS is ruled out by the very close values of α_G determined by in-plane and out-of-plane FMR (with geometry suppressing TMS) measurements. According to the behavior of ΔH vs f in Fig. 2(a), the $Co_{0.98}Ir_{0.02}$ film is most likely to contain TMS among the
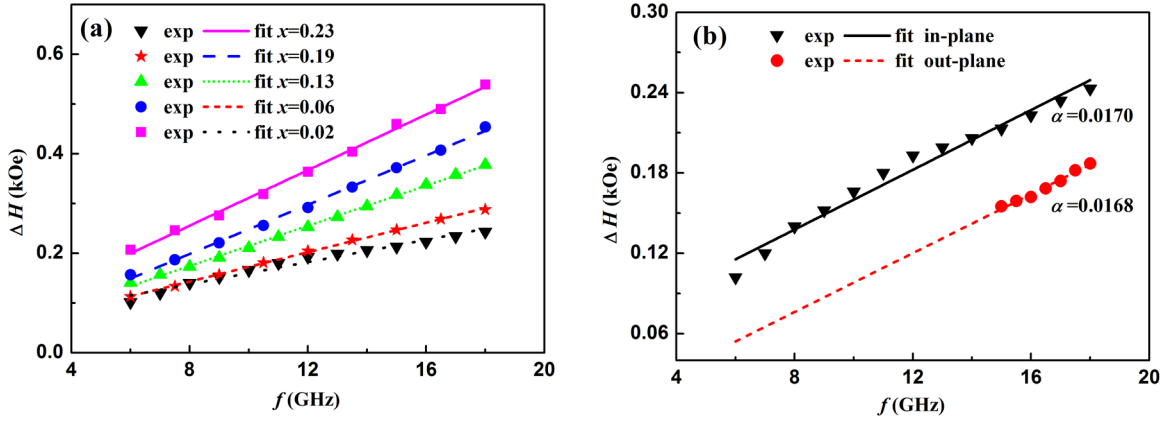
FIG. 2. Relation between the resonance linewidth ΔH and frequency obtained at $T = 300$ K with a magnetic field parallel to the (a) in-plane hard axis of the $Co_{1-x}Ir_x$ films and (b) out-of-plane and in-plane hard axes of the $Co_{0.98}Ir_{0.02}$ film.

$Co_{1-x}Ir_x$ films. However, the difference in α_G is observed to be only 0.0002, as shown in Fig. 2(b). Second, interfacial contributions are disregarded, considering that the thickness of the CoIr samples is significantly larger than the thickness that could enable visible spins to be pumped into adjacent layers (as well as the thickness that could induce interfacial TMS)

FIG. 3. (a) Composition dependence of α_G for the $Co_{1-x}Ir_x$ films. The ξ^2 (b), γM_s (c), and D_{Ef} (d) for the $Co_{1-x}Ir_x$ alloys and pure hcp Co with the lattice constants of the P-$6m2$ $Co_{1-x}Ir_x$ supercells. The parameters (pink crosses) of pure hcp Co at each x represent the value obtained under the lattice constants of the corresponding $Co_{1-x}Ir_x$ supercell.

[2,10,27,28]. Third, the α_{rad} and α_{eddy} can also be ignored, as their values are estimated to be smaller than 0.0016 and 0.0001 according to the reported radiative and eddy-current damping equation, respectively [1,29]. Therefore, α_G is approximately equal to α_{int}, and the impact parameters of α_{int} give rise to the linear variation in α_G.

We then clarify the x dependence of α_{int} for CoIr alloys. In the disordered CoIr alloys, Ir impurities have strong scattering efficiency, owing to the reported results about the $3d$ transition metals with $5d$ impurities, as well as to the peak in Ir-DOS near E_f of CoIr alloy [30,31]. Consequently, the impact on the variation of damping from grain boundaries and microstructural defects would be limited in comparison to the contributions within the grains [28,30]. The dominance of phonon-driven (atomic-displacement) scattering at room temperature and/or impurity-driven (chemical disorder) scattering may effectively diminish the roles of microstructural defects in Gilbert damping [28]. Moreover, the films present equivalent structural quality. Therefore, we focus on the influence of ξ, γM_s, D_{Ef}, and lattice constants. The electron-lattice scattering rate is almost fixed and excluded, considering the invariant residual resistivity with x.

First-principles calculation of the ξ, γM_s, and D_{Ef} of the $Co_{1-x}Ir_x$ alloys and hcp Co (with the lattice constants of the P-$6m2$ $Co_{1-x}Ir_x$ supercells) were performed. The main results, shown in Figs. 3(b)–3(d), indicate that the relative variation in ξ^2 is more significant than that in the other parameters. This variation is closely related to that in α_G, although each of the parameters undergoes a consistent linear variation. Specifically, the stable lattice expansion (only 1.5% as mentioned above) is not expected to impact the change in α_G. This is because ξ, γM_s, D_{Ef} of hcp Co under the lattice constants of $Co_{1-x}Ir_x$ [indicated by the pink crosses in Figs. 3(b)–3(d)] are altered insignificantly by the changes in the lattice constants. α_{int} is inversely proportional to γM_s if the other parameters are fixed [17,30,32]; however, the relative reduction in γM_s is only 22% and is insufficient to induce the relative increment of 153% in α_G. Hence, γM_s cannot be the overarching factor responsible for the increase in α_G. The D_{Ef} has a 33% relative increment. The α_σ, as a part of α_G, is proportional to D_{Ef} [13,16] hence D_{Ef} would play a role in the increase of α_G. However, the increase in
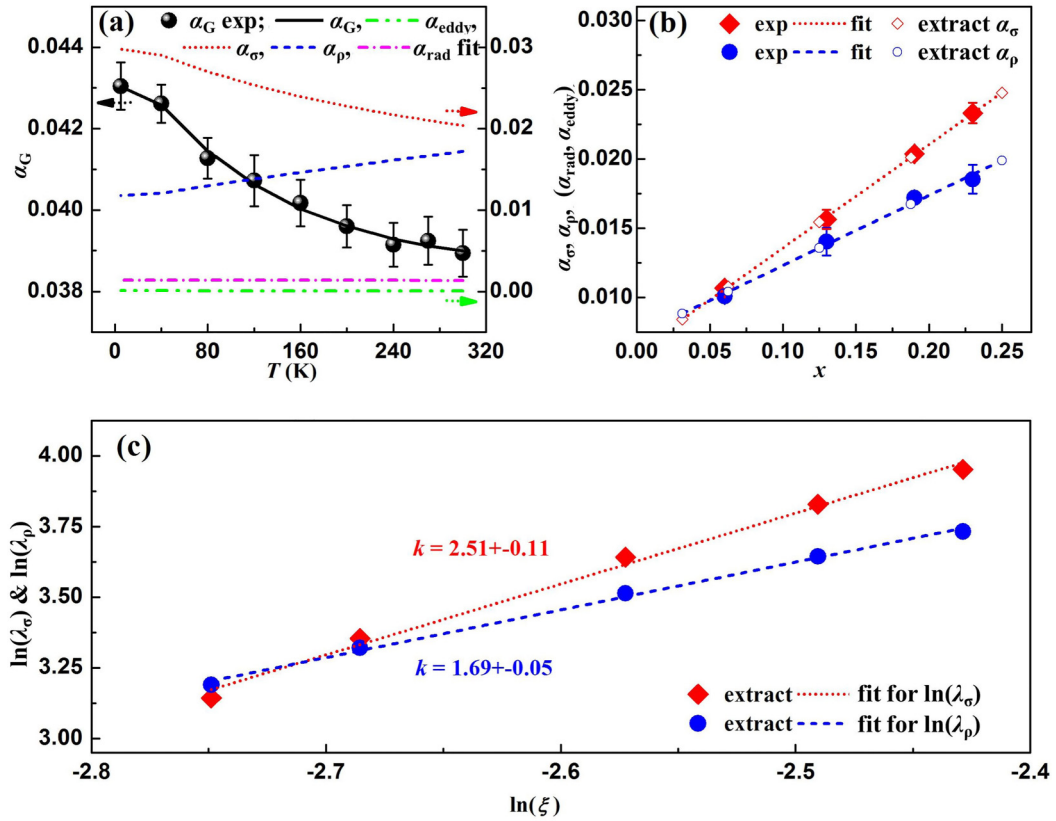
FIG. 4. (a) Temperature dependence of α_G (left scale label) and its constituents $\alpha_\sigma(T)$, $\alpha_\rho(T)$, $\alpha_{eddy}(T)$, and $\alpha_{rad}(T)$ (right scale label) for the $Co_{0.81}Ir_{0.19}$ film. The round dots indicate the experimental results, and the curves are the fitted results. (b) Composition dependence of α_σ and α_ρ for the $Co_{1-x}Ir_x$ films. The results obtained according to Eq. (5) and their linear fittings are displayed with solid dots and dashed lines, respectively. The hollow dots are data points extracted from the linear fittings. (c) Relationships between $\ln(\lambda_\sigma)$ and $\ln(\xi)$ (shown in red) and between $\ln(\lambda_\rho)$ and $\ln(\xi)$ (shown in blue) for the $Co_{1-x}Ir_x$ films. The solid dots are the results transformed from the extracted data points, and the curves are the corresponding linear fittings. k refers to the slopes of the linear fittings.

D_{Ef} is regarded as a result of the changes in ξ rather than the band filling effect or/and the lattice distortion. The band filling effect is not significant as Co and Ir atoms contain the same number of outer d electrons. The calculated D_{Ef} of pure hcp Co with the lattice constants of $Co_{1-x}Ir_x$ [pink crosses in Fig. 3(d)] manifests that changing the lattice parameter alone does not induce remarkable changes in D_{Ef}. In addition, the impact of D_{Ef} on α_G would be diluted, as the intraband scattering (inducing the α_σ) would have been suppressed by disorder in our polycrystalline films [2,13,30]. In view of the above, compared with the other parameters, the ξ has the most pronounced effect on α_G. Hence the linear variation in α_{int} of the $Co_{1-x}Ir_x$ films is most likely to originate from the linear increase in ξ^2, similar to the reported quadratic scaling of α_{int} with ξ in $L10$ FePdPt films [7].

C. Conductivity-like damping α_σ and resistivity-like damping α_ρ

The dependence of α_{int} on ξ^2 was observed in this system and in $L10$ FePd$_{1-x}$Pt$_x$ films at room temperature [7]. As the α_{int} is governed by α_σ at low temperature and by α_ρ at high temperature according to the torque correlation model [1], the prediction that α_ρ is proportional to ξ^2 is preliminarily confirmed [7,16]. However, the ratio of $\alpha_\rho/\alpha_\sigma$ is reported to be 1.25–3.6 [1,2,33], indicating the non-negligible con-

tribution of α_σ even at room temperature. Hence, to further understand the ξ dependence of α_{int}, it is essential to clarify the scaling exponents of α_σ and α_ρ with ξ.

To this end, variable-temperature FMR measurements were performed. The $\Delta H - f$ results were fitted at each temperature (T) to obtain the temperature dependence of α_G. Taking $Co_{0.81}Ir_{0.19}$ as an example, as shown in Fig. 4(a), the α_G increases with decreasing temperature, in agreement with the published results [1,2]. The small proportion extrinsic damping (less than 10% as mentioned above) would be inessential to this increase at low temperature. For instance, we are not aware of any mechanism that enhances two-magnon scattering with decreasing temperature [2]. In particular, as M_s is almost constant across the measured temperature range, the dipolar interactions that induce TMS should not change much with temperature [2]. However, we still discard the $Co_{0.98}Ir_{0.02}$ film in the following discussion because its TMS, despite being small, is more notable than in the other films. Furthermore, assuming a uniform magnetization profile and excitation field, the contributions of α_{rad} and α_{eddy} to $\alpha_G(T)$ can be estimated via [1,2,29]

$$\alpha_{rad}(T) = \frac{\gamma \mu_0^2 M_s(T) dl}{8 Z_0 w}, \tag{3}$$

$$\alpha_{\text{eddy}}(T) = \frac{1}{12\rho(T)}\gamma\mu_0^2 M_s(T)d^2, \qquad (4)$$

where μ_0 is the permeability of vacuum and d is the thickness of the CoIr layer. Further, Z_0, w, and l are the waveguide impedance, width of the waveguide, and length of the sample on the waveguide, respectively. Here, we set $Z_0 = 50\ \Omega$ and $l/w = 50$ for fitting. The α_{eddy} and α_{rad} are estimated to be smaller than 0.0002 and 0.0017 even at low temperature, respectively.

Phenomenologically, the temperature dependence of α_{int} ($= \alpha_G - \alpha_{\text{rad}} - \alpha_{\text{eddy}}$) can be fitted with a combination of the conductivity-like term ($\alpha_\sigma(T)$) and resistivity-like term [$\alpha_\rho(T)$] [2]:

$$\alpha_{\text{int}}(T) = \alpha_\sigma \frac{\sigma(T)}{\sigma(300\ \text{K})} + \alpha_\rho \frac{\rho(T)}{\rho(300\ \text{K})}, \qquad (5)$$

where $\sigma(T)$ [inversely proportional to $\rho(T)$] is the temperature-dependent conductivity, whereupon the α_σ and α_ρ of the $Co_{1-x}Ir_x$ films can be extracted by fitting the experimental $\alpha_G(T)$ with $\alpha_\sigma(T)$, $\alpha_\rho(T)$, $\alpha_{\text{rad}}(T)$, and $\alpha_{\text{eddy}}(T)$ included. As an example, Fig. 4(a) presents the fitting results of $\alpha_G(T)$, $\alpha_\sigma(T)$, $\alpha_\rho(T)$, $\alpha_{\text{rad}}(T)$, and $\alpha_{\text{eddy}}(T)$ of the $Co_{0.81}Ir_{0.19}$ film. Obviously, the fitting agrees well with the experimental results of α_G. From the fitting, the experimental values of $\alpha_\sigma(T)$ and $\alpha_\rho(T)$ can be obtained. Damping at room temperature is useful for applications of various spintronic and electromagnetic devices, thus we preferentially focus on the data at $T = 300$ K (unless otherwise noted). The compositional dependence of α_σ and α_ρ is plotted with solid red diamonds and blue dots in Fig. 4(b), respectively. Both α_σ and α_ρ increase linearly with increasing x, whereas the former increases faster. The ratios of $\alpha_\rho/\alpha_\sigma$ are 0.945, 0.897, 0.844, and 0.795 for $x = 0.06$, 0.13, 0.19, and 0.23, respectively. These ratios are smaller than those of Fe films and this is attributed to the disordered structure and the significantly slower changes in $\rho(T)$ [1,2]. To facilitate subsequent discussion, the value of α_σ (α_ρ) at the Ir compositions used in our calculation (hollow points) was extracted from the linear fitting of the experimental α_σ (α_ρ) results.

Generally, both the α_σ and α_ρ are inversely proportional to γM_s, which is separated from the other parameters, as the Landau-Lifshitz damping rate $\lambda_G = \alpha_G\gamma M_s$ [17,30,32]. Despite the small reduction in γM_s, we still exclude its effect by transforming α_σ (α_ρ) into the corresponding Landau-Lifshitz damping rate λ_σ (λ_ρ) so as to contrast with the reported theoretical results where fixed parameters are specified except for ξ. Subsequently, $\ln(\lambda_\sigma)$ and $\ln(\lambda_\rho)$ versus $\ln(\xi)$ were calculated, and the corresponding results were displayed in Fig. 4(c). Both the $\ln(\lambda_\sigma)$ and $\ln(\lambda_\rho)$ are linearly dependent on $\ln(\xi)$. The slopes are estimated to be 2.51 ± 0.11 and 1.69 ± 0.05 for the $\ln(\lambda_\sigma)$-$\ln(\xi)$ and $\ln(\lambda_\rho)$-$\ln(\xi)$ lines, respectively. The ratio of the two slopes is 1.48. Similarly, we also estimated the slopes for the results under $T = 5$ K, and the corresponding value are 2.42 ± 0.11 and 1.77 ± 0.06, respectively. These results indicate that the scaling exponent of α_σ (α_ρ) with ξ in the disordered $Co_{1-x}Ir_x$ alloys approximately agrees with Gilmore's prediction that α_σ (α_ρ) is proportional to ξ^3 (ξ^2) in pure Fe, Co, and Ni metals [16].

The smaller value of the scaling exponents in the $Co_{1-x}Ir_x$ system may be attributable to the ignored extrinsic damping contributions (e.g., TMS) and the underrated impact factors (e.g., microstructural defects) [2]. In addition, the ξ^3-x and ξ^2-x curves of the CoIr system do not differ significantly in shape. Hence, a greater range of variations in α_G and ξ with small changes in other related parameters is required to verify the scaling exponents.

We then turned to clarifying the origin of the greater magnitude of the ξ scaling exponent of α_σ than that of α_ρ. The α_{int} depends on the product of the integral over the spectral functions (related to DOS) and the squared torque matrix elements (related to ξ), according to the torque correlation model [8,16,34]. By treating the SO interaction as a perturbation and expanding the states in the powers of ξ, the squared torque matrix elements (which contain two submechanisms: spin flips and orbital excitations) are shown to have contributions of the order of ξ^2 and higher [16]. Gilmore suggests that the ξ^3 dependence of α_σ (in pure Fe, Co, and Ni metals) is due to the zero return of the spin flip in the ξ^2 order of the intraband (only with pure spin states) [16]. Because, in pure metals with the prominent atomic-displacement scattering processes, the spin flips are more significant than orbital excitations, the zero return of the spin flip weakens the ξ^2 term and leads to the dominance of the ξ^3 term in the intraband case [16,30]. However, in the CoIr system, impurity-driven scattering is considerably more pronounced than atomic-displacement scattering [16,30]. Thus, the orbital excitations are more significant than spin flips, resulting in the comparable strength of the ξ^2 term for α_σ and α_ρ. Consequently, the zero contribution of the spin flip to the ξ^2 order is not sufficient to induce this great difference in the ξ scaling exponents of the two types of damping in the CoIr system.

We note that the change in D_{Ef} may actually be the leading cause of the greater ξ scaling exponent of α_σ in the CoIr system. The integral over the spectral functions is essentially proportional to D_{Ef} in α_σ [10,16], whereas it is unnecessary to consider the correlation between α_ρ and D_{Ef} (which has not been observed) owing to the complicated influence of the spectral overlap [16]. In Gilmore's prediction [16], the ξ was artificially tuned from zero to full strength, which would cause a significant variation in the split of DOS between the majority and minority spin states and hence D_{Ef}. However, the influence of this variation in D_{Ef} on α_σ was not discussed. In the CoIr alloys, the 33% relative increment in D_{Ef} mainly originates from the change in ξ (as discussed above). If the influence of D_{Ef} on α_σ is deducted, the scaling exponent will be 1.57 ± 0.21, in accordance with that of α_ρ. Therefore, we argue that the difference in the ξ dependence of the α_σ and α_ρ for the CoIr system mainly comes from the variation in D_{Ef} induced by ξ.

IV. CONCLUSION

In this study, we investigated the variation and mechanism of damping as a function of the composition in oriented hcp $Co_{1-x}Ir_x$ films. To this end, we employed FMR measurements and first-principles calculations. The Gilbert damping rate α_G exhibits a significant linear increase with increasing Ir concentration x. This is most likely due to the dominance

of the SO parameter ξ, considering the significantly smaller changes in other leading parameters and the stable high resistivity of the system. Based on the temperature dependence of α_G, the conductivity-like (α_σ) and resistivity-like (α_ρ) Gilbert damping rate were separated out, and were found to increase linearly with different slopes with increasing x, whereupon we have experimentally demonstrated the approximate cubic (quadratic) scaling of α_σ (α_ρ) with ξ in the disordered CoIr alloy. The greater ξ scaling exponent of α_σ than that of α_ρ is derived from the non-negligible variation in D_{Ef} induced by ξ, rather than the finding that the contribution of the ξ^2 term of the squared torque matrix elements for the intraband is smaller than that for the interband. The latter is considered to be the main reason for this difference in pure $3d$ ferromagnetic metals. However, further studies that entail greater variations in α_G and ξ but small changes in other related parameters would be required to verify these scaling exponents. The present results provide deeper insight into the damping mechanism in magnetic metallic materials. Furthermore, they provide theoretical and experimental bases on which to design and fabricate new magnetic alloys with tailored damping properties.

[1] Z. Xu, K. Zhang, and J. Li, Disentangling intrinsic and extrinsic gilbert damping, Phys. Rev. B **104**, 224404 (2021).

[2] B. Khodadadi, A. Rai, A. Sapkota, A. Srivastava, B. Nepal, Y. Lim *et al.*, Conductivitylike Gilbert Damping Due to Intraband Scattering in Epitaxial Iron, Phys. Rev. Lett. **124**, 157201 (2020).

[3] M. Arora, E. K. Delczeg-Czirjak, G. Riley, T. J. Silva, H. T. Nembach, O. Eriksson, and J. M. Shaw, Magnetic Damping in Polycrystalline Thin-Film Fe-V Alloys, Phys. Rev. Appl. **15**, 054031 (2021).

[4] X. Liu, W. Zhang, M. J. Carter, and G. Xiao, Ferromagnetic resonance and damping properties of CoFeB thin films as free layers in MgO-based magnetic tunnel junctions, J. Appl. Phys. **110**, 033910 (2011).

[5] M. Strungaru, S. Ruta, R. F. L. Evans, and R. W. Chantrell, Model of Magnetic Damping and Anisotropy at Elevated Temperatures: Application to Granular FePt Films, Phys. Rev. Appl. **14**, 014077 (2020).

[6] Y. S. Hou and R. Q. Wu, Strongly Enhanced Gilbert Damping in 3 D Transition-Metal Ferromagnet Monolayers in Contact with the Topological Insulator Bi_2Se_3, Phys. Rev. Appl. **11**, 054032 (2019).

[7] P. He, X. Ma, J. W. Zhang, H. B. Zhao, G. Lüpke, Z. Shi, and S. M. Zhou, Quadratic Scaling of Intrinsic Gilbert Damping with Spin-Orbital Coupling in $L1_0$ FePdPt Films: Experiments and *Ab Initio* Calculations, Phys. Rev. Lett. **110**, 077203 (2013).

[8] K. Gilmore, Y. U. Idzerda, and M. D. Stiles, Identification of the Dominant Precession-Damping Mechanism in Fe, Co, and Ni by First-Principles Calculations, Phys. Rev. Lett. **99**, 027204 (2007).

[9] A. Brataas, Y. Tserkovnyak, and G. E. W. Bauer, Scattering Theory of Gilbert Damping, Phys. Rev. Lett. **101**, 037207 (2008).

[10] M. A. W. Schoen, D. Thonig, M. L. Schneider, T. J. Silva, H. T. Nembach, O. Eriksson, O. Karis, and J. M. Shaw, Ultra-low magnetic damping of a metallic ferromagnet, Nat. Phys. **12**, 839 (2016).

[11] P. Zhang, S. Li, J. Yao, H. Zhang, X. Feng, Q. Zhang, J. Cao, X. Fan, and D. Xue, Variation of effective damping with temperature in permalloy/Gd heterostructures, Phys. Rev. B **102**, 174439 (2020).

[12] S. J. Xu, J. Y. Shi, Y. S. Hou, Z. Zheng, H. B. Zhao, R. Q. Wu, S. M. Zhou, Z. Shi, and W. J. Fan, Tuning of the intrinsic magnetic damping parameter in epitaxial CoNi(001) films: Role of the band-filling effect, Phys. Rev. B **100**, 024403 (2019).

[13] D. A. Smith, A. Rai, Y. Lim, T. Q. Hartnett, A. Sapkota, A. Srivastava *et al.*, Magnetic Damping in Epitaxial Iron Alloyed with Vanadium and Aluminum, Phys. Rev. Appl. **14**, 034042 (2020).

[14] C. Scheck, L. Cheng, I. Barsukov, Z. Frait, and W. E. Bailey, Low Relaxation Rate in Epitaxial Vanadium-Doped Ultrathin Iron Films, Phys. Rev. Lett. **98**, 117601 (2007).

[15] J. O. Rantschler, R. D. McMichael, A. Castillo, A. J. Shapiro, W. F. Egelhoff, B. B. Maranville, D. Pulugurtha, A. P. Chen, and L. M. Connors, Effect of 3d, 4d, and 5d transition metal doping on damping in permalloy thin films, J. Appl. Phys. **101**, 033911 (2007).

[16] K. Gilmore, Y. U. Idzerda, and M. D. Stiles, Spin-orbit precession damping in transition metal ferromagnets (Invited), J. Appl. Phys. **103**, 07D303 (2008).

[17] V. Kamberský, Spin-orbital Gilbert damping in common magnetic metals, Phys. Rev. B **76**, 134416 (2007).

[18] J. Stohr and H. C. Siegmann, *Magnetism from Fundamentals to Nanoscale Dynamics* (Springer, Berlin, Heidelberg, New York, 2010).

[19] P. Blaha, K. Schwarz, G. Madsen, D. Kvasnicka, and J. Luitz, WIEN2k, *An Augmented Plane Wave Plus Local Orbitals Program for Calculating Crystal Properties User's* (Techn. Universitat, Vienna, Austria, 2017).

[20] J. P. Perdew, K. Burke, and M. Ernzerhof, Generalized Gradient Approximation Made Simple, Phys. Rev. Lett. **77**, 3865 (1996).

[21] See Supplemental Material at http://link.aps.org/supplemental/10.1103/PhysRevB.108.094424 for additional information on calculation of the displayed properties, surface appearance and static magnetic properties, FMR spectra and gyromagnetic ratio, and measurement and fitting for the temperature dependence of Gilbert damping rate. It also contains Refs. [2,3,24–26].

[22] X. Li, K. W. Lin, H. T. Liang, P. L. Liu, W. C. Lo, D. L. Cortie, F. Klose, J. Van Lierop, L. Li, and P. W. T. Pong, The effects of post-deposition ion-beam bombardment with oxygen on the Co surface in modifying the magnetic properties of Co thin films, Microelectron. Eng. **152**, 41 (2016).

[23] O. Kazakova, D. Erts, T. A. Crowley, J. S. Kulkarni, and J. D. Holmes, Temperature dependence of magnetization reversal in Co and Fe_3O_4 nanowire arrays, J. Magn. Magn. Mater. **286**, 171 (2005).

[24] B. K. Kuanr, V. Veerakumar, A. V. Kuanr, R. E. Camley, and Z. Celinski, Effect of temperature on the ferromagnetic-resonance field and line width of epitaxial Fe thin films, IEEE Trans. Magn. **45**, 4015 (2009).

[25] S. Zhang, T. Fu, T. Wang, X. Fan, M. Gao, Z. Li, and F. Li, Gyromagnetic ratio of oriented hcp $Co_{1-x}Ir_x$ soft magnetic films, J. Phys. D: Appl. Phys. **54**, 505005 (2021).

[26] S. J. Lee, C. C. Tsai, H. Cho, M. Seo, T. Eom, W. Nam, Y. P. Lee, and J. B. Ketterson, Hysteretic characteristics of low-field microwave absorption of a Co thin film, J. Appl. Phys. **106**, 063922 (2009).

[27] H. Chen, X. Fan, W. Wang, H. Zhou, Y. S. Gui, C. M. Hu, and D. Xue, Electric detection of the thickness dependent damping in $Co_{90}Zr_{10}$ thin films, Appl. Phys. Lett. **102**, 202410 (2013).

[28] S. Wu, D. A. Smith, P. Nakarmi, A. Rai, M. Clavel, M. K. Hudait *et al.*, Room-temperature intrinsic and extrinsic damping in polycrystalline Fe thin films, Phys. Rev. B **105**, 174408 (2022).

[29] M. A. W. Schoen, J. M. Shaw, H. T. Nembach, M. Weiler, and T. J. Silva, Radiative damping in waveguide-based ferromagnetic resonance measured via analysis of perpendicular standing spin waves in sputtered permalloy films, Phys. Rev. B. **92**, 184417 (2015).

[30] S. Mankovsky, D. Ködderitzsch, G. Woltersdorf, and H. Ebert, First-principles calculation of the Gilbert damping parameter via the linear response formalism with application to magnetic transition metals and alloys, Phys. Rev. B **87**, 014430 (2013).

[31] S. Zhang, H. Pang, L. Hai, W. Li, T. Wang, and F. Li, First-principles study of the easy-plane magnetocrystalline anisotropy in bulk hcp $Co_{1-X}Ir_X$, J. Appl. Phys. **126**, 083907 (2019).

[32] H. Ebert, S. Mankovsky, D. Ködderitzsch, and P. J. Kelly, Ab Initio Calculation of the Gilbert Damping Parameter Via the Linear Response Formalism, Phys. Rev. Lett. **107**, 066603 (2011).

[33] V. Haspot, P. Noël, J. P. Attané, L. Vila, M. Bibes, A. Anane, and A. Barthélémy, Temperature dependence of the Gilbert damping of $La_{0.7}Sr_{0.3}MnO_3$ thin films, Phys. Rev. Mater. **6**, 024406 (2022).

[34] V. Kamberský, FMR linewidth and disorder in metals, Czech. J. Phys. **34**, 1111 (1984).